

# MonoTAKD: Teaching Assistant Knowledge Distillation for Monocular 3D Object Detection

Hou-I Liu<sup>1</sup> Christine Wu<sup>2</sup> Jen-Hao Cheng<sup>2</sup> Wenhao Chai<sup>2</sup> Shian-Yun Wang<sup>3</sup>

Gaowen Liu<sup>4</sup> Jenq-Neng Hwang<sup>2</sup> Hong-Han Shuai<sup>1</sup> Wen-Huang Cheng<sup>5</sup>

<sup>1</sup>National Yang Ming Chiao Tung University, Hsinchu City, Taiwan

<sup>2</sup>University of Washington, Seattle, WA, USA

<sup>3</sup>University of Southern California, Los Angeles, CA, USA

<sup>4</sup>Cisco Systems, Inc., San Jose, CA, USA

<sup>5</sup>National Taiwan University, Taipei City, Taiwan

k39967.c@nycu.edu.tw, hhshuai@nycu.edu.tw, wenhuang@csie.ntu.edu.tw

{wuc29, andyhci, wchai, hwang}@uw.edu, shianyun@usc.edu, gaoliu@cisco.com

## Abstract

Monocular 3D object detection (Mono3D) holds noteworthy promise for autonomous driving applications owing to the cost-effectiveness and rich visual context of monocular camera sensors. However, depth ambiguity poses a significant challenge, as it requires extracting precise 3D scene geometry from a single image, resulting in suboptimal performance when transferring knowledge from a LiDAR-based teacher model to a camera-based student model. To address this issue, we introduce Monocular Teaching Assistant Knowledge Distillation (MonoTAKD) to enhance 3D perception in Mono3D. Our approach presents a robust camera-based teaching assistant model that effectively bridges the representation gap between different modalities for teacher and student models, addressing the challenge of inaccurate depth estimation. By defining 3D spatial cues as residual features that capture the differences between the teacher and the teaching assistant models, we leverage these cues into the student model, improving its 3D perception capabilities. Experimental results show that our MonoTAKD achieves state-of-the-art performance on the KITTI3D dataset. Additionally, we evaluate the performance on nuScenes and KITTI raw datasets to demonstrate the generalization of our model to multi-view 3D and unsupervised data settings. Our code will be available at <https://github.com/hoiliu-0801/MonoTAKD>.

## 1. Introduction

Monocular 3D object detection (Mono3D) attracts great attention in autonomous driving with its cost-effective monocular camera sensors [9, 15, 26, 53, 55]. One widely

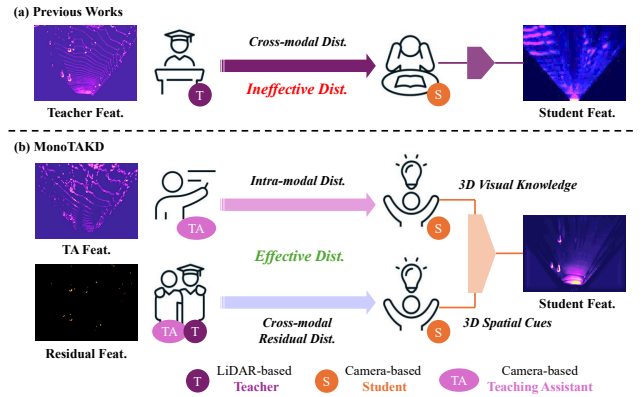


Figure 1. Comparison between previous methods and MonoTAKD (Ours). Previous works [7, 12] face a significant challenge in the distillation process due to a substantial gap in feature representation. Our MonoTAKD incorporates intra-modal distillation and cross-modal residual distillation to enhance the learning across this feature representation gap. We visualize the BEV features and the residual features of each model, which are highlighted in orange. Best view with zoom-in and color.

used approach for improving 3D detection performance is to leverage depth maps as auxiliary supervision. For example, MonoPGC [45] and MonoDTR [15] apply an additional depth branch to predict depth maps and aggregate them with the visual features by a transformer-based decoder. However, the accuracy of depth maps estimated from a single image remains restricted for the camera-based models, primarily due to the absence of stereoscopic data, which is critical to understanding the geometry of 3D scenes [10, 51].

To enhance the extraction and comprehension of 3D information, a promising alternative to depth-guided ap-

proaches is to utilize the cross-modal distillation [12, 54]. This kind of approach enables models trained with images to acquire 3D information directly from LiDAR data. For instance, CMKD [12] and UniDistill [54] employ a LiDAR-based model (teacher) to extract critical 3D information and distill this knowledge into the camera-based model (student) through the bird’s eye view (BEV) distillation [6]. Nevertheless, the feature representations from different modalities are inherently distinct, which causes ineffective distillation and restricts the performance of the camera-based student [16, 42], as depicted in Fig. 1 (a).

To minimize the global distance between cross-modal features, recent approaches involve using an adaptation module [12, 43] or applying regularization [17] to map the cross-modal features. Unfortunately, due to the significant differences between the two modalities, learning an effective alignment remains challenging. Therefore, we introduce a novel *Teaching Assistant Knowledge Distillation framework, MonoTAKD*. First, we introduce a camera-based model as the teaching assistant (TA) model to guide the student model with robust 3D visual knowledge, as shown at the top of Fig. 1 (b). The TA model directly accesses the ground truth (GT) depth map and integrates visual features from the camera-based model to reconstruct optimal BEV features, referred to as 3D visual knowledge. The TA model has two primary functions: (1) By providing the optimal BEV features to the student model, it mitigates the distortion brought by inaccurate depth estimation in the camera-based model. (2) This approach facilitates effective distillation through intra-modal distillation (IMD), as the feature representation gap is smaller within the same modality (camera image) compared to cross-modal scenarios (LiDAR points and camera image) [46].

Specifically, we attempt to make the BEV features of the student model close to those of the TA model<sup>1</sup>. As such, the 3D perception of the student model is enhanced without relying on LiDAR data. It is worth noting that there is no distillation relationship between the teacher and TA models, as visual and LiDAR features serve as independent learning targets. Additionally, we use end-to-end rather than multi-step [29] distillation during training.

Even when the student model perfectly replicates the BEV features of the TA model through IMD, a feature representation gap still exists between the replicated BEV features and those of the teacher model. This gap arises because the monocular image inherently lacks certain 3D spatial cues that are exclusive to the LiDAR modality. To this end, we formulate these 3D spatial cues by computing the feature difference in BEV features between the teacher and teaching assistant models. Consequently, we define this feature difference as the residual features that are distilled

into the student model through the proposed cross-modal residual distillation (CMRD), as illustrated at the bottom of Fig. 1 (b). This approach empowers the student model to concentrate on learning the crucial 3D spatial cues instead of being compelled to replicate the complex entirety of BEV features from the LiDAR-based teacher. We believe that learning the key differences (residual features) between the LiDAR and camera model is pivotal for the camera-based student to enhance its 3D perception.

Since the camera-based models struggle with capturing 3D spatial cues due to their limited understanding of 3D geometry, we propose a spatial alignment module (SAM) to refine the student’s BEV features. This module enhances the 3D spatial cues in those features by capturing global information and compensating spatial shifts, thus better capturing the 3D representation from the residual features. Notably, SAM is an optional module with an acceptable FLOPs overhead. Even without SAM, our MonoTAKD still significantly surpasses the state-of-the-art methods by a noticeable margin.

Our contributions are three-fold:

- Our MonoTAKD utilizes intra-modal distillation to transfer rich 3D visual knowledge, and applies cross-modal residual distillation to convey essential 3D spatial cues to the student model.
- We develop a SAM to garner rich global information and to compensate for the spatial shift caused by feature distortion. Also, we design an FFM to expertly integrate features from different modalities, resulting in a more comprehensive 3D representation.
- Experimental results show that MonoTAKD achieves state-of-the-art performance on the KITTI 3D detection benchmark. To demonstrate its generalizability, we validate MonoTAKD on the nuScenes and KITTI raw datasets, confirming its effectiveness in multi-view camera and unsupervised data settings.

## 2. Related Work

### 2.1. LiDAR-based 3D Object Detection.

LiDAR sensors have been widely used in 3D object detection since point clouds can represent precise 3D environmental information [37]. For example, point-based methods [34, 36] take raw points as input and process the point-wise features with a sizeable multi-layer perceptron. Voxel-based methods [8, 44, 49] convert point clouds into voxel grids and extract the voxelized features through 3D sparse convolution layers. Although LiDAR-based 3D object detection methods have proven to be high-performing techniques, LiDAR systems are expensive, making them impractical for autonomous driving.

<sup>1</sup>We conduct knowledge distillation of student and TA models in a unified BEV space to facilitate 3D detection.

## 2.2. Depth-guided Mono3D.

Monocular 3D object detection methods offer a promising low-cost solution for autonomous driving applications. Depth-guided methods [9, 35, 40, 53] leverage depth information to help 3D perception. Early methods [9, 40] implemented an off-the-shelf depth estimator to predict depth maps, which are then integrated into visual features through a fusion module. CaDDN [35] predicts depth distribution bins with image features to reconstruct a 3D frustum feature. However, image features lack the understanding of 3D scene geometry, leading to unreliable depth predictions.

## 2.3. Semi-supervised Mono3D.

Semi-supervised Mono3D typically incorporate unlabeled data to training dataset, increasing the quantity of valuable data and thereby enhancing the model’s robustness. LPCG [32] conducts instant segmentation on images and uses a heuristic algorithm to create 3D pseudo labels. Mix-Teaching [50] exploits the pre-trained model to generate pseudo labels and pastes them into the image background regions to increase the number of instances in unlabeled data. Yet, increasing training data also brings significant training time, and the generated noisy pseudo-labels may hurt the performance.

## 2.4. Cross-modal distillation for Mono3D.

Several works [7, 12, 42, 46, 54] apply cross-modal distillation to Mono3D. For example, MonoDistill [7] uses a camera-based model as the teacher model to process the sparse depth map and transfer inferred 3D information to the student model through feature and logit distillation. To enhance 3D information, CMKD [12] and DistillBEV [43] employ a LiDAR-based model to extract enriched 3D features from the LiDAR point cloud. Then, they perform the BEV distillation to transfer this knowledge from the LiDAR modality to the camera modality.

Nevertheless, prior research in KD has predominantly focused on using a single modality teacher, which could impede the comprehensive acquisition of 3D knowledge. A camera-based student often struggles to gain this knowledge due to substantial differences in feature representation. Cross-modal feature alignment typically relies on a simple adaptation module, which may be insufficient for effectively bridging this gap [12, 43]. In contrast, our MonoTAKD employs intra-modal distillation to effectively transfer 3D visual knowledge and introduces cross-modal residual distillation to convey essential 3D spatial cues.

# 3. Method

## 3.1. Overview

Our MonoTAKD framework, as illustrated in Fig. 2, comprises a pre-trained LiDAR-based model as the teacher  $\mathcal{T}$

and two camera-based models, serving as the teaching assistant  $\mathcal{A}$  and student  $\mathcal{S}$ . These three models communicate by propagating BEV features, enabling knowledge distillation during training to enhance the performance of Mono3D tasks. The core innovation of our architecture is the integration of two distillation techniques: intra-modal distillation (IMD), which enriches 3D visual knowledge, and cross-modal residual distillation (CMRD), which provides 3D spatial cues. To further enrich the BEV feature representation in  $\mathcal{S}$ , we introduce a spatial alignment module (SAM) to refine its BEV features. Finally, a feature fusion module (FFM) is applied to unify features from both distillation branches of  $\mathcal{S}$ , ensuring a more cohesive 3D representation.

## 3.2. LiDAR-based Teacher

To exploit the 3D representation and to enhance the 3D perception capabilities of the student model  $\mathcal{S}$ , we use a pre-trained LiDAR-based model [49] as the teacher model  $\mathcal{T}$  to directly encode 3D information for distillation. As shown in the top block of Fig. 2,  $\mathcal{T}$  voxelizes the unordered point cloud data captured from LiDAR into voxel grids  $v$ , passing through the 3D backbone to obtain voxel features. We then employ height compression [12], denoted as  $\phi$ , to embed these voxel features into the BEV space, forming the BEV feature  $F^T \in \mathbb{R}^{H \times W \times C}$ . The process to derive the BEV feature from  $\mathcal{T}$  can be formulated as

$$F^T = \phi(\psi(v)), \quad (1)$$

where  $\psi$  represents a series of sparse convolution layers.

## 3.3. Camera-based Teaching Assistant

Cross-modal distillation in Mono3D [7, 12] is challenging due to the knowledge heterogeneity between modalities, and relying on solely complex adaptation modules [17, 43] for feature alignment proves insufficient. To overcome the limitations of direct cross-modal distillation, we introduce a negotiator, *i.e.*, the TA model, to expertly bridge the teacher and student models, enabling effective knowledge transfer via IMD. To alleviate knowledge heterogeneity, we select a camera-based model [35] as the TA model  $\mathcal{A}$ , which shares the same modality as the student model  $\mathcal{S}$ . We further ensure feature alignment is tractable by jointly projecting the latent representations into BEV space, allowing  $\mathcal{S}$  to efficiently obtain relevant 3D visual knowledge from  $\mathcal{A}$ .

As depicted in the middle block of Fig. 2,  $\mathcal{A}$  processes a monocular image input by extracting visual features through a 2D backbone (ResNet50), including a  $1 \times 1$  convolutional layer to adjust the channel dimensions. Unlike previous depth-guided methods [15, 53],  $\mathcal{A}$  operates on the ground truth depth maps  $d \in \mathbb{R}^{H \times W \times D}$  by computing the outer product with the resulting visual feature  $f$ , where  $D$  stands for the number of discrete depth bins. This approach effectively injects accurate depth information into

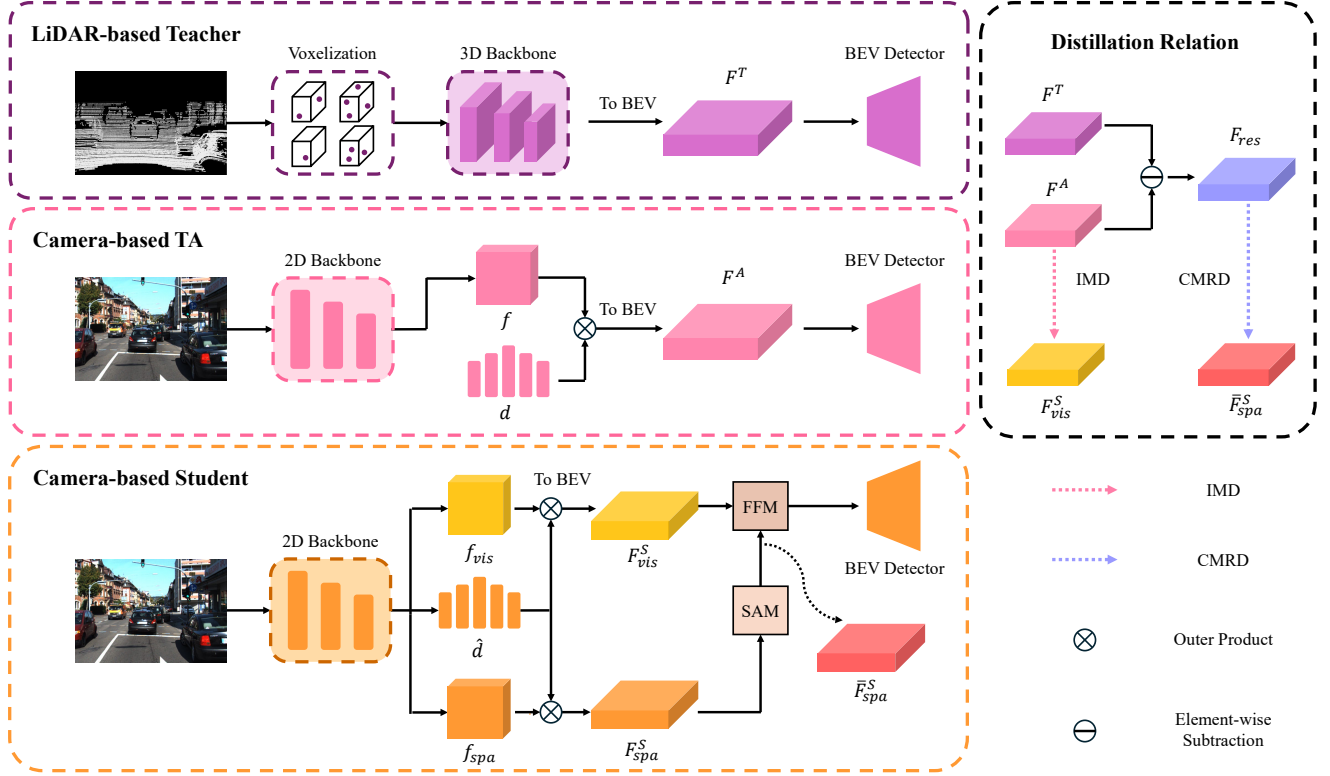


Figure 2. Overall architecture of the MonoTAKD. The top, middle, and bottom rows show the architecture of the LiDAR-based teacher, the camera-based teaching assistant (TA), and a camera-based student. We design the intra-modal distillation (IMD) and the cross-modal residual distillation (CMRD) processes to guide the camera-based student. In addition, a spatial alignment module (SAM) and a feature fusion module (FFM) are employed to improve the BEV feature representation.

the TA model, reducing feature distortion from inaccurate depth estimations and enabling the TA model to achieve performance closer to the optimal levels expected from a camera-based model. Formally, we formulate the BEV feature from  $\mathcal{A}$  as

$$F^A = \phi(f \otimes d), \quad (2)$$

where  $d$  represents the ground truth depth maps,  $\otimes$  denotes the outer product,  $\phi$  is the projection function similar to (Eq. 1) with minor modifications (e.g. interpolation [12]), and  $1 \times 1$  convolution for arranging the desired dimension. Hereafter, we refer to  $F^A$  as 3D visual knowledge, which serves as one of the learning targets for the student model.

### 3.4. Camera-based Student

The primary goal in designing the student model is to accurately detect objects in monocular images while developing a robust understanding of 3D scenes. Based on this perspective, we adopt a camera-based model that closely mirrors  $\mathcal{A}$ . Specifically, we use the same 2D backbone to extract the visual feature and incorporate a learnable depth estimator to predict depth map  $\hat{d}$ . After processing the image through the 2D backbone,  $\mathcal{S}$  employs two separate heads to generate

distinct visual features (different weights), denoted as  $f_{vis}$  and  $f_{spa}$ . By splitting the features into two branches,  $f_{vis}$  focuses on learning 3D visual knowledge from  $\mathcal{A}$ , while  $f_{spa}$  is dedicated to learning 3D spatial cues from the relation of  $\mathcal{A}$  and  $\mathcal{T}$ . This dual-branch structure optimizes the student’s capacity to understand both visual and spatial information crucial for robust 3D perception. Together with the predicted depth map  $\hat{d}$ , the paired representations go through the projection described in (Eq. 2), resulting in BEV features  $F_{vis}^S$  and  $F_{spa}^S$ .

With the established BEV features ( $F^T$ ,  $F^A$ ,  $F_{vis}^S$ ,  $F_{spa}^S$ ) from the three models, the following sections detail the distillation, refinement, and fusion processes that drive comprehensive integration of 3D information across modalities.

**Intra-modal distillation.** Since the camera-based  $\mathcal{A}$  and  $\mathcal{S}$  share the same modality, their feature representation gap is expected to be smaller than the gap observed in direct cross-modal distillation between  $\mathcal{T}$  and  $\mathcal{S}$ . This similarity in representation makes intra-modal distillation (IMD) a more effective strategy for knowledge transfer. In our approach, we leverage the BEV features  $F^A$  as 3D visual knowledge and distill it into the BEV features  $F_{vis}^S$ .



The IMD process is optimized by minimizing the mean square error (MSE) between corresponding feature representations, which can be expressed as

$$\mathcal{L}_{IMD} = \text{MSE}(F_{vis}^S, F^A). \quad (3)$$

**Spatial Alignment Module.** To strengthen the student’s ability to capture 3D information, we introduce a Spatial Alignment Module (SAM) to refine its BEV features. We denote  $\bar{F}_{spa}^S$  as the enhanced BEV features obtained by processing  $F_{spa}^S$  through SAM. As illustrated in Fig. 3, SAM captures extensive global information and mitigates spatial feature misalignment through Atrous and Deformable convolutions. More precisely, Atrous Spatial Pyramid Pooling (ASPP) [4] expands the receptive fields using multiscale dilated convolutions, encouraging the model to capture richer 3D information. On the other hand, Deformable convolutions [56] adjust spatial offsets to address distortions in BEV features caused by inaccurate depth estimations, thus reducing spatial misalignment in feature representation. Additionally, we incorporate a SENet-like block [13] within SAM to recalibrate features adaptively along the channel dimension, enhancing the model’s sensitivity to essential 3D cues. This well-designed module allows SAM to enhance feature alignment and effectively integrate valuable spatial information into the student’s BEV features.

**Cross-modal Residual Distillation.** While we designate the BEV features of the TA model as the learning target for the student model in (Eq. 3), they still fall short of fully capturing the 3D spatial richness provided by LiDAR. Although incorporating GT depth maps into the TA model narrows such a gap, a discrepancy remains due to the lack of precise 3D spatial cues intrinsic to LiDAR data. Unlike previous cross-modal distillation methods, which require the student model to mimic the raw features from the teacher, our MonoTAKD identifies the missing 3D spatial cues as residual features, providing an additional learning objective. Particularly, the distillation of residual features covers vital spatial information and enhances the 3D perception of the student model. The loss function can be defined as

$$\mathcal{L}_{CMRD} = \text{MSE}(\bar{F}_{spa}^S, F_{res}), \quad (4)$$

where  $F_{res} = F^T \ominus F^A$  represents the residual features. We note that  $F_{res}$  is calculated as the difference of BEV features between  $\mathcal{T}$  and  $\mathcal{A}$  by element-wise subtraction and is binarized by a predefined threshold to suppress background noise and emphasize essential spatial regions (see Fig. 4).

**Feature Fusion Module.** To aggregate two BEV features from the student model, i.e.,  $F_{vis}^S$  and  $\bar{F}_{spa}^S$ , we apply a Feature Fusion Module (FFM) to integrate their expertise in both visual and spatial 3D information. Specifically, we begin by fusing features  $F_{vis}^S$  and  $\bar{F}_{spa}^S$  (the enhanced feature by SAM) using element-wise addition. This combined

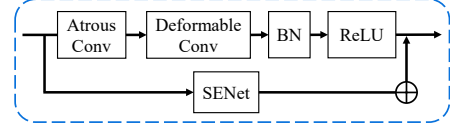


Figure 3. Spatial Alignment Module (SAM). SAM cascades the Atrous and Deformable convolutions to learn the alignment of BEV features. SENet is adopted for channel attention.

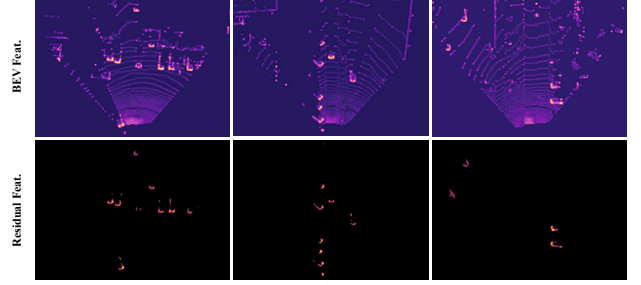


Figure 4. Comparing the BEV features ( $F^T$ ) from the teacher model with the residual features ( $F_{res}$ ) reveals that our residuals effectively capture essential 3D spatial cues, emphasizing critical information over less important elements, such as ripples and background noise seen in the BEV LiDAR features.

representation is then processed through two convolutional layers. The fusion process can be simplified as

$$F^S = \text{FFM}(F_{vis}^S \oplus \bar{F}_{spa}^S). \quad (5)$$

The resulting fused feature  $F^S$  is subsequently fed into a BEV detector [22] for 3D object detection, generating the prediction for object localization and recognition.

### 3.5. Loss Function

Our proposed MonoTAKD framework is end-to-end trained with an objective function  $\mathcal{L}_{total}$  that combines multiple components to effectively guide KD. This total loss function can be expressed as

$$\mathcal{L}_{total} = \mathcal{L}_{IMD} + \mathcal{L}_{CMRD} + \mathcal{L}_{logit}, \quad (6)$$

where the first two terms are introduced in (Eq. 3) and (Eq. 4). The last term in (Eq. 6) is logit distillation for the student model, formulated as

$$\mathcal{L}_{logit} = \mathcal{L}_{cls} + \mathcal{L}_{reg}, \quad (7)$$

where the former term represents the classification loss accomplished by quality focal loss [23]. The latter utilizes the Smooth L1 loss for the bounding box regression for precise localization. Both classification and regression losses are computed over the predictions from the teacher model.

Table 1. Experimental results on the KITTI *test* set for the Car category. We use **bold** and underline to indicate the best and the second-best results, respectively. †denotes the KD-based methods.

Method	Venue	Extra Data	$AP_{3D}$			$AP_{BEV}$		
			Easy	Mod.	Hard	Easy	Mod.	Hard
DDMP-3D [39]	CVPR 21	Pre-trained Depth	19.71	12.78	9.80	28.08	17.89	13.44
DD3D [30]	ICCV 21		23.22	16.34	14.20	30.98	22.56	20.03
Kinematic3D [1]	ECCV 20	Temporal	19.07	12.72	9.17	26.69	17.52	13.10
Dfm [1]	ECCV 22		22.94	16.82	14.65	31.71	22.89	19.97
CaDDN [35]	CVPR 21	LiDAR Auxiliary	19.17	13.41	11.46	27.94	18.91	17.19
MonoDTR [15]	CVPR 22		21.99	15.39	12.73	28.59	20.38	17.14
MonoNerd [47]	ICCV 23		22.75	17.13	15.63	31.13	23.46	20.97
MonoPGC [45]	ICRA 23		24.68	17.17	14.14	32.50	23.14	20.30
OccupancyM3D [33]	CVPR 24		25.55	17.02	14.79	35.38	24.18	21.37
MonoDistill† [7]	ICLR 22	None	22.97	16.03	13.60	31.87	22.59	19.72
Cube R-CNN [2]	CVPR 23		23.59	15.01	12.56	31.70	21.20	18.43
MonoUNI [18]	NeurIPS 23		24.75	16.73	13.49	33.28	23.05	19.39
MonoATT [55]	CVPR 23		24.72	<u>17.37</u>	15.00	<u>36.87</u>	<u>24.42</u>	<u>21.88</u>
MonoDETR [53]	ICCV 23		25.00	16.47	13.58	33.60	22.11	18.60
CMKD† [12]	ECCV 22		25.09	16.99	<u>15.30</u>	33.69	23.10	20.67
ADD† [46]	AAAI 23		<u>25.61</u>	16.81	13.79	35.20	23.58	20.08
MonoCD [48]	CVPR 24		25.53	16.59	14.53	33.41	22.81	19.57
<b>MonoTAKD</b>	-	None	<b>27.91</b>	<b>19.43</b>	<b>16.51</b>	<b>38.75</b>	<b>27.76</b>	<b>24.14</b>

## 4. Experiments

### 4.1. Datasets and Evaluation Metrics

**KITTI3D.** The KITTI 3D detection dataset [11] is a widely used benchmark in the field of autonomous driving. It consists of 7,481 training images and 7,518 testing images with synchronized LiDAR point cloud. Following the data split provided by [5], the training images are further split into two groups: 3,712 images and 3,769 images as the train and val sets, respectively. We report the 3D detection performance  $AP_{3D}$  and the BEV detection performance  $AP_{BEV}$  with 40 recall positions [38]. Our detection results include three difficulty levels: easy, moderate, and hard.

**nuScenes.** The nuScenes dataset [3] includes 1,000 multi-modal video sequences, 700 for training, 150 for validation, and 150 for testing. It offers synchronized sensor data streams collected with 6 cameras and a 32-beam LiDAR sampled at 20Hz, covering the 360-degree field of view. We utilize nuScenes Detection Score (NDS) and the mean Average Precision (mAP) as the primary evaluation metrics. Due to space limits, other dataset descriptions and implementation details are provided in the supplementary material.

### 4.2. Main Results

**Results on KITTI3D.** We demonstrate the effectiveness of our MonoTAKD on the KITTI test set for the Car category in Table 1. First, MonoTAKD outperforms the second-best result by +2.30, +2.06, and +1.21 in  $AP_{3D}$ , by +1.88, +3.34, +2.26 in  $AP_{BEV}$  under easy, moderate, and hard difficulty levels, respectively. When compared to CMKD, the top-performing KD-based method, MonoTAKD, consistently surpasses CMKD, achieving +2.82, +2.44, +1.21

Table 2. Experimental results on the nuScenes *val* set. We use **bold** to indicate the best results in each setting.

Method	Modality	Backbone	NDS†	mAP†
PETrv2 [28]	C	R50	0.456	0.349
P2D [19]	C	R50	0.486	0.374
PGD [41]	C	R101	0.428	0.369
MonoDETR [53]	C	R101	0.526	0.423
BEVFormer [25]	C	R50	0.423	0.352
+BEVDistill [6]	$L \rightarrow C$	R50	0.457	0.386
+DistillBEV [43]	$L \rightarrow C$	R50	0.476	0.367
+STXD [17]	$L \rightarrow C$	R50	0.481	0.374
+TAKD (Ours)	$L \rightarrow C$	R50	<b>0.490</b>	<b>0.392</b>
BEVFormer	C	R101	0.445	0.374
+BEVDistill	$L \rightarrow C$	R101	0.468	0.389
+DistillBEV	$L \rightarrow C$	R101	0.545	0.446
+STXD	$L \rightarrow C$	R101	0.543	0.440
+TAKD (Ours)	$L \rightarrow C$	R101	<b>0.558</b>	<b>0.451</b>
BEVDepth [24]	C	R50	0.440	0.317
+STXD	$L \rightarrow C$	R50	0.483	0.371
+DistillBEV	$L \rightarrow C$	R50	0.510	0.403
+LabelDistill [20]	$L \rightarrow C$	R50	0.528	0.419
+TAKD (Ours)	$L \rightarrow C$	R50	<b>0.537</b>	<b>0.430</b>
BEVDepth	C	R101	0.535	0.412
+DistillBEV	$L \rightarrow C$	R101	0.547	0.450
+LabelDistill	$L \rightarrow C$	R101	0.553	0.451
+TAKD (Ours)	$L \rightarrow C$	R101	<b>0.564</b>	<b>0.466</b>

improvements in  $AP_{3D}$  across all difficulty levels. Moreover, we observe a significant performance gain over all proceeding depth-guided methods. For instance, with respect to MonoDETR, our model achieves a notable increase of +2.93 (21.58%) in  $AP_{3D}$  under the hard level.

Our successful performance lies in incorporating intra-modal distillation (IMD) and cross-modal residual distillation (CMRD), which provide the student model with rich

Table 3. Compared the effect of distillation losses using various teacher, TA, and student models. \* indicates the insertion of the ground truth depth. We use **bold** and underline to indicate the best and the second-best results, respectively.

Model Types			$AP_{3D}$			$AP_{BEV}$		
Teacher model	TA model	Student model	Easy	Mod.	Hard	Easy	Mod.	Hard
None	None	CaDDN	23.57	16.31	13.84	30.28	21.53	18.90
CenterPoint [52]	CaDDN*	CaDDN	27.06	19.38	17.50	35.66	26.03	23.09
PointPillar [22]	CaDDN*	CaDDN	31.28	20.80	17.58	<u>42.21</u>	28.48	<u>25.73</u>
Second [49]	CaDDN*	CaDDN	<b>34.36</b>	<b>22.61</b>	<b>19.88</b>	<b>42.86</b>	<b>29.41</b>	<b>26.47</b>
CenterPoint	MonoDETR*	CaDDN	26.56	18.84	16.46	34.62	25.85	22.29
PointPillar	MonoDETR*	CaDDN	28.11	20.00	17.24	40.21	27.10	24.65
Second	MonoDETR*	CaDDN	30.74	20.35	17.69	41.75	28.95	24.80
None	None	MonoDETR	28.84	20.61	16.38	37.86	26.95	22.80
CenterPoint	MonoDETR*	MonoDETR	30.78	21.17	18.41	39.73	27.22	24.69
PointPillar	MonoDETR*	MonoDETR	31.25	21.47	<u>18.57</u>	38.68	27.16	24.83
Second	MonoDETR*	MonoDETR	<u>33.18</u>	<u>21.97</u>	18.55	41.98	28.43	25.24

3D visual knowledge and crucial 3D spatial cues. This combined approach enhances both the semantic information and understanding of 3D scene geometry for the student model. Note that additional performance metrics for other classes (Pedestrian and Cyclist) and visualizations are provided in the supplementary material.

**Results on nuScenes.** We further evaluate MonoTAKD on the nuScenes val set, as shown in Table 2. For consistent and effective distillation, we use CenterPoint as the LiDAR-based teacher and employ the same architecture for both the TA and student models, as validated in Table 3.

Our results show significant improvements in NDS and mAP for both BEVFormer and BEVDepth. This reveals the potential to scale our feature distillation losses from monocular to multi-view camera applications, which showcases the generalizability of our approach. Additionally, we observe higher performance using BEVDepth as the student model due to its similarity to CenterPoint’s dense prediction head, enhancing the effectiveness of logit distillation.

### 4.3. Ablation study

For easier comparison with other methods, we conduct ablation studies on the KITTI val set for the Car category, using ResNet50 as the backbone for the TA and student models.

**Generalization Study with Different Teacher and Teaching Assistant Models.** We employ CaDDN and MonoDETR without distillation techniques as the baseline models in this experiment. The findings in Table 3 suggest utilizing the same model for the TA and student models. As such, the implementation is simpler and more generalizable than creating a custom TA model for each detector. Moreover, we observe that distilling knowledge across heterogeneous architectures (transformer to CNN) may be ineffective due to substantial differences in feature encoding. Our study demonstrates that MonoTAKD consistently boosts performance under the guidance of various LiDAR-based teacher and camera-based TA models. Ultimately, Second is se-

Table 4. Effectiveness of different feature distillation losses.

Settings	Loss			$AP_{3D}$		
	IMD	CMD	CMRD	Easy	Mod.	Hard
1				24.35	16.16	13.44
2	✓			31.11	20.24	16.91
3		✓		28.22	18.29	15.10
4	✓	✓		30.73	19.88	16.43
5	✓		✓	<b>34.36</b>	<b>22.61</b>	<b>19.88</b>

lected as our LiDAR-based teacher, with CaDDN serving as both the TA and student models.

**Effectiveness of Different Feature Distillation.** We present the effect of each feature distillation loss on MonoTAKD’s performance in terms of  $AP_{3D}$  and  $AP_{BEV}$ , as shown in Table 4. Setting 1 represents the baseline performance of the camera-based student without any distillation loss guidance. Cross-modal distillation (CMD) refers to the camera-based student learning directly from the LiDAR BEV features. Settings 2 and 3 investigate the effectiveness of distillation between IMD and CMD. The student model performs better with IMD because the distillation is across a narrower feature representation gap than CMD.

Comparing the performance between settings 4 and 5, focusing on learning 3D spatial cues (residual features) within the LiDAR BEV feature proves more beneficial over the exhaustive replication of all 3D information provided by the LiDAR modality (CMD). For instance, the student model can prioritize discerning the precise shape and position of foreground objects while avoiding unnecessary attention to the background noise, which could impede the understanding of 3D scene geometry. As a result, setting 5 (MonoTAKD) outperforms baseline in  $AP_{3D}$  by +10.1, +6.45, and +6.44 for the easy, moderate, and hard difficulty levels, respectively. For this experiment, the feature fusion module (FFM) is removed for settings 1-3, as they do not require BEV feature fusion.

Additionally, we report training curves for each feature distillation loss at the moderate level, as depicted in Fig. 5. When comparing the training curves between IMD and

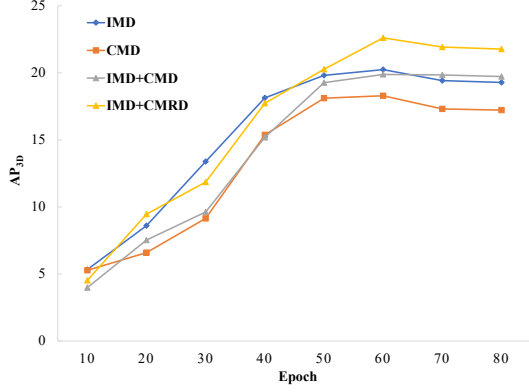


Figure 5. Convergence curves of different feature distillation on the KITTI *val* set. The x-axis denotes the number of epochs, and the y-axis denotes  $AP_{3D}$  for the Car category under the moderate level. Note the performance at 60 epochs is highlighted, representing the peak  $AP_{3D}$  across all settings.

Table 5. Effectiveness of the components in SAM. DConv. indicates the deformable convolution.

Components			$AP_{3D}$		
ASPP	DConv.	SENet	Easy	Mod.	Hard
✓			31.36	20.80	16.53
	✓		32.28	21.45	17.18
✓	✓		32.46	21.51	17.99
✓	✓	✓	33.19	21.81	18.23
✓	✓	✓	<b>34.36</b>	<b>22.61</b>	<b>19.88</b>

Table 6. Efficiency analysis of MonoTAKD.

Model	Parameters (M)	FLOPs (G)	$AP_{3D}$		
			Easy	Moderate	Hard
MonoNeRD [47]	83.0	356.57	20.64	15.44	13.99
DD3D [30]	80.3	163.00	26.23	21.21	18.83
MonoDETR [53]	47.4	57.51	28.84	20.61	16.38
CMKD [12]	<b>45.1</b>	<b>41.32</b>	23.53	16.33	14.44
MonoTAKD-Lite	<b>45.1</b>	<b>41.32</b>	31.11	20.24	16.91
MonoTAKD	47.8	44.90	<b>34.36</b>	<b>22.61</b>	<b>19.88</b>

CMD, CMD consistently shows lower  $AP_{3D}$  values. It suggests IMD is more effective than CMD, leading to a smaller feature representation gap within the same modality.

Finally, our IMD+CMRD (MonoTAKD) remarkably outperforms IMD+CMD throughout the training process. This observation indicates that the student model greatly benefits from learning residual features rather than learning from the entirety of LiDAR BEV features, thereby enhancing the effectiveness of cross-modal distillation. Notably, each feature distillation loss converges within approximately 60 epochs, demonstrating that the proposed feature distillation losses and modules, such as SAM, do not extend training time. Furthermore, all experiments can be conducted on a consumer-grade GPU with only 12GB VRAM, indicating that our method imposes minimal impact on training costs.

**Effectiveness of the Components of the Spatial Alignment Module.** Table 5 illustrates the performance boost brought by each component of SAM. The baseline is the MonoTAKD with IMD and CMRD but without SAM. With the combination of all components, MonoTAKD improves +3.00, +2.81, and +3.35 in  $AP_{3D}$  in three difficulty levels, highlighting the effectiveness of our SAM in learning spatial shifts in regions both near and far, reducing the feature representation gap between the LiDAR and camera. **Efficiency Analysis.** To further evaluate the practicality of the model at the application level, we tabulate the FLOPs and parameters of state-of-the-art Mono3D methods in Table 6. By leveraging the KD-based framework, CMKD reaches a substantial reduction in parameters and FLOPs compared to depth-guided methods, DD3Dv2 and MonoDETR. However, distilling knowledge across the large feature gap between teacher and student models results in a notable AP drop. To ensure a fair comparison with CMKD, we remove both SAM and FFM modules from our student model, creating a lightweight version, MonoTAKD-lite, which is aligned with the architecture of CMKD (CaDDN). MonoTAKD-Lite effectively mitigates the performance drop while remaining a compact student model. This version is how we compute the performance of IMD solely. Notably, even without the SAM module, our method demonstrates a clear performance gain over state-of-the-art approaches, such as MonoDETR, offering higher  $AP_{3D}$ , reduced FLOPs, and fewer parameters. The analysis of the backbone choices can be found in the supplementary.

## 5. Discussion

To garner 3D perception from a 2D image, recent Mono3D methods can be categorized into four major strategies: (1) Extra training data. This method leverages LiDAR-generated auxiliary labels, such as depth maps [15, 45, 47], occupancy labels [33], temporal data [1, 17], to improve the training process. (2) Depth-guided. Using additional depth estimator [9, 40, 53, 55] or pre-training on additional depth datasets [30, 31] to improve depth estimation. (3) Cross-modal. Leveraging LiDAR-based teacher to camera-based student [12, 20, 43, 54]. Fair comparisons are challenged by heterogeneous experimental settings and varying model architectures. The lack of standardized efficiency metrics (FLOPs, parameter counts) makes it difficult to assess the true cost-benefit and trade-offs. We advocate for future work to report such metrics to enable fair comparisons across architectures and backbones.

## 6. Conclusion

In this paper, we propose a novel teaching assistant knowledge distillation for Mono3D (MonoTAKD) to improve the cross-modal distillation’s effectiveness. Specifically, we observe that the camera-based student model struggles to learn



3D information due to a significant feature representation gap between LiDAR and camera modalities. We alleviate this impediment by employing a camera-based teaching assistant model to deliver robust visual knowledge through intra-modal distillation. To enhance the 3D perception of the student model, we formulate the LiDAR-exclusive 3D spatial cues as residual features and then distill them to the student model through cross-modal residual distillation. As a result, MonoTAKD establishes a new state-of-the-art benchmark on the KITTI 3D detection dataset. With its accurate yet cost-effective attributes, MonoTAKD poses a promising solution for autonomous driving applications.

## References

- [1] Garrick Brazil, Gerard Pons-Moll, Xiaoming Liu, and Bernt Schiele. Kinematic 3d object detection in monocular video. In *ECCV*, pages 135–152, 2020.
- [2] Garrick Brazil, Abhinav Kumar, Julian Straub, Nikhila Ravi, Justin Johnson, and Georgia Gkioxari. Omni3d: A large benchmark and model for 3d object detection in the wild. In *CVPR*, pages 13154–13164, 2023.
- [3] Holger Caesar, Varun Bankiti, Alex H. Lang, Sourabh Vora, Venice Erin Liong, Qiang Xu, Anush Krishnan, Yu Pan, Giancarlo Baldan, and Oscar Beijbom. nuscenes: A multimodal dataset for autonomous driving. In *CVPR*, pages 11618–11628, 2020.
- [4] Liang-Chieh Chen, George Papandreou, Iasonas Kokkinos, Kevin Murphy, and Alan L. Yuille. Deeplab: Semantic image segmentation with deep convolutional nets, atrous convolution, and fully connected crfs. *TPAMI*, 40(4), 2018.
- [5] Xiaozhi Chen, Kaustav Kundu, Yukun Zhu, Andrew G Berneshawi, Huimin Ma, Sanja Fidler, and Raquel Urtasun. 3d object proposals for accurate object class detection. In *NeurIPS*, 2015.
- [6] Zehui Chen, Zhenyu Li, Shiquan Zhang, Liangji Fang, Qin-hong Jiang, and Feng Zhao. Bevdistill: Cross-modal bev distillation for multi-view 3d object detection. In *ICLR*, 2023.
- [7] Zhiyu Chong, Xinzhu Ma, Hong Zhang, Yuxin Yue, Haojie Li, Zhihui Wang, and Wanli Ouyang. Monodistill: Learning spatial features for monocular 3d object detection. In *ICLR*, 2022.
- [8] Jiajun Deng, Shaoshuai Shi, Peiwei Li, Wengang Zhou, Yanyong Zhang, and Houqiang Li. Voxel r-cnn: Towards high performance voxel-based 3d object detection. In *Proceedings of the AAAI conference on artificial intelligence*, pages 1201–1209, 2021.
- [9] Mingyu Ding, Yuqi Huo, Hongwei Yi, Zhe Wang, Jianping Shi, Zhiwu Lu, and Ping Luo. Learning depth-guided convolutions for monocular 3d object detection. In *CVPRW*, pages 1000–1001, 2020.
- [10] Huan Fu, Mingming Gong, Chaohui Wang, Kayhan Batmanghelich, and Dacheng Tao. Deep ordinal regression network for monocular depth estimation. In *CVPR*, pages 2002–2011, 2018.
- [11] Andreas Geiger, Philip Lenz, Christoph Stiller, and Raquel Urtasun. Vision meets robotics: The kitti dataset. *The International Journal of Robotics Research*, 32(11):1231–1237, 2013.
- [12] Yu Hong and et al. Cross-modality knowledge distillation network for monocular 3d object detection. In *ECCV*, pages 87–104, 2022.
- [13] Jie Hu, Li Shen, and Gang Sun. Squeeze-and-excitation networks. In *CVPR*, pages 7132–7141, 2018.
- [14] Junjie Huang, Guan Huang, Zheng Zhu, and Dalong Du. Bevdet: High-performance multi-camera 3d object detection in bird-eye-view. *arXiv preprint arXiv:2112.11790*, 2021.
- [15] Kuan-Chih Huang, Tsung-Han Wu, Hung-Ting Su, and Winston H. Hsu. Monodtr: Monocular 3d object detection with depth-aware transformer. In *CVPR*, pages 4012–4021, 2022.
- [16] Peixiang Huang, Li Liu, Renrui Zhang, Song Zhang, Xinli Xu, Baichao Wang, and Guoyi Liu. Tig-bev: Multi-view bev 3d object detection via target inner-geometry learning. *arXiv preprint arXiv:2212.13979*, 2022.
- [17] Sujin Jang, Dae Ung Jo, Sung Ju Hwang, Dongwook Lee, and Daehyun Ji. Stxd: structural and temporal cross-modal distillation for multi-view 3d object detection. *NeurIPS*, 36, 2024.
- [18] Jia Jinrang, Zhenjia Li, and Yifeng Shi. Monouni: A unified vehicle and infrastructure-side monocular 3d object detection network with sufficient depth clues. In *NeurIPS*, pages 11703–11715, 2023.
- [19] Sanmin Kim, Youngseok Kim, In-Jae Lee, and Dongsuk Kum. Predict to detect: Prediction-guided 3d object detection using sequential images. In *ICCV*, pages 18057–18066, 2023.
- [20] Sanmin Kim, Youngseok Kim, Sihwan Hwang, Hyeonjun Jeong, and Dongsuk Kum. Labeldistill: Label-guided cross-modal knowledge distillation for camera-based 3d object detection. In *ECCV*, pages 19–37, 2025.
- [21] Jason Ku, Alex D Pon, and Steven L Waslander. Monocular 3d object detection leveraging accurate proposals and shape reconstruction. In *CVPR*, pages 11867–11876, 2019.
- [22] Alex H. Lang, Sourabh Vora, Holger Caesar, Lubing Zhou, Jiong Yang, and Oscar Beijbom. Pointpillars: Fast encoders for object detection from point clouds. In *CVPR*, pages 12697–12705, 2019.
- [23] Xiang Li, Wenhui Wang, Lijun Wu, Shuo Chen, Xiaolin Hu, Jun Li, Jinhui Tang, and Jian Yang. Generalized focal loss: Learning qualified and distributed bounding boxes for dense object detection. *NeurIPS*, 33:21002–21012, 2020.
- [24] Yinhao Li, Zheng Ge, Guanyi Yu, Jinrong Yang, Zengran Wang, Yukang Shi, Jianjian Sun, and Zeming Li. Bevdepth: Acquisition of reliable depth for multi-view 3d object detection. In *AAAI*, pages 1477–1485, 2023.
- [25] Zhiqi Li, Wenhui Wang, Hongyang Li, Enze Xie, Chonghao Sima, Tong Lu, Yu Qiao, and Jifeng Dai. Bevformer: Learning bird’s-eye-view representation from multi-camera images via spatiotemporal transformers. In *ECCV*, pages 1–18, 2022.
- [26] Xianpeng Liu, Nan Xue, and Tianfu Wu. Learning auxiliary monocular contexts helps monocular 3d object detection. In *AAAI*, pages 1810–1818, 2022.

- [27] Yingfei Liu, Tiancai Wang, Xiangyu Zhang, and Jian Sun. Petr: Position embedding transformation for multi-view 3d object detection. In *ECCV*, pages 531–548, 2022.
- [28] Yingfei Liu, Junjie Yan, Fan Jia, Shuailin Li, Aqi Gao, Tiancai Wang, and Xiangyu Zhang. Petr2: A unified framework for 3d perception from multi-camera images. In *ICCV*, pages 3262–3272, 2023.
- [29] Seyed Iman Mirzadeh, Mehrdad Farajtabar, Ang Li, Nir Levine, Akihiro Matsukawa, and Hassan Ghasemzadeh. Improved knowledge distillation via teacher assistant. In *AAAI*, pages 5191–5198, 2020.
- [30] Dennis Park, Rares Ambrus, Vitor Guizilini, Jie Li, and Adrien Gaidon. Is pseudo-lidar needed for monocular 3d object detection? In *ICCV*, pages 3142–3152, 2021.
- [31] Dennis Park, Jie Li, Dian Chen, Vitor Guizilini, and Adrien Gaidon. Depth is all you need for monocular 3d detection. In *ICRA*, pages 7024–7031, 2023.
- [32] Liang Peng, Fei Liu, Zhengxu Yu, Senbo Yan, Dan Deng, Zheng Yang, Haifeng Liu, and Deng Cai. Lidar point cloud guided monocular 3d object detection. In *ECCV*, pages 123–139, 2022.
- [33] Liang Peng, Junkai Xu, Haoran Cheng, Zheng Yang, Xiaopei Wu, Wei Qian, Wenxiao Wang, Boxi Wu, and Deng Cai. Learning occupancy for monocular 3d object detection. In *CVPR*, pages 10281–10292, 2024.
- [34] Charles R. Qi, Hao Su, Kaichun Mo, and Leonidas J. Guibas. Pointnet: Deep learning on point sets for 3d classification and segmentation. In *CVPR*, pages 652–660, 2017.
- [35] Cody Reading, Ali Harakeh, Julia Chae, and Steven L. Waslander. Categorical depth distribution network for monocular 3d object detection. In *CVPR*, pages 8555–8564, 2021.
- [36] Shaoshuai Shi, Xiaogang Wang, and Hongsheng Li. Point-rcnn: 3d object proposal generation and detection from point cloud. In *CVPR*, pages 770–779, 2019.
- [37] Shaoshuai Shi, Chaoxu Guo, Li Jiang, Zhe Wang, Jianping Shi, Xiaogang Wang, and Hongsheng Li. Pv-rcnn: Point-voxel feature set abstraction for 3d object detection. In *CVPR*, pages 1–14, 2020.
- [38] Andrea Simonelli, Samuel Rota Buló, Lorenzo Porzi, Manuel Lopez-Antequera, and Peter Kotschieder. Disentangling monocular 3d object detection. In *ICCV*, pages 1991–1999, 2019.
- [39] Li Wang, Liang Du, Xiaoqing Ye, Yanwei Fu, Guodong Guo, Xiangyang Xue, Jianfeng Feng, and Li Zhang. Depth-conditioned dynamic message propagation for monocular 3d object detection. In *CVPR*, pages 454–463, 2021.
- [40] Li Wang, Liang Du, Xiaoqing Ye, Yanwei Fu, Guodong Guo, Xiangyang Xue, Jianfeng Feng, and Li Zhang. Depth-conditioned dynamic message propagation for monocular 3d object detection. In *CVPR*, pages 454–463, 2021.
- [41] Tai Wang, Xinge Zhu, Jiangmiao Pang, and Dahua Lin. Probabilistic and geometric depth: Detecting objects in perspective. In *CoRL*, pages 1475–1485, 2021.
- [42] Zeyu Wang, Dingwen Li, Chenxu Luo, Cihang Xie, and Xiaodong Yang. Distillbev: Boosting multi-camera 3d object detection with cross-modal knowledge distillation. In *ICCV*, pages 8637–8646, 2023.
- [43] Zeyu Wang, Dingwen Li, Chenxu Luo, Cihang Xie, and Xiaodong Yang. Distillbev: Boosting multi-camera 3d object detection with cross-modal knowledge distillation. In *ICCV*, pages 8637–8646, 2023.
- [44] Hai Wu, Chenglu Wen, Shaoshuai Shi, Xin Li, and Cheng Wang. Virtual sparse convolution for multimodal 3d object detection. In *CVPR*, pages 21653–21662, 2023.
- [45] Zizhang Wu, Yuanzhu Gan, Lei Wang, Guilian Chen, and Jian Pu. Monopgc: Monocular 3d object detection with pixel geometry contexts. In *ICRA*, pages 4842–4849, 2023.
- [46] Zizhang Wu, Yunzhe Wu, Jian Pu, Xianzhi Li, and Xiaoquan Wang. Attention-based depth distillation with 3d-aware positional encoding for monocular 3d object detection. In *AAAI*, pages 2892–2900, 2023.
- [47] Junkai Xu, Liang Peng, Haoran Cheng, Hao Li, Wei Qian, Ke Li, Wenxiao Wang, and Deng Cai. Mononerf: Nerf-like representations for monocular 3d object detection. In *ICCV*, pages 6814–6824, 2023.
- [48] Longfei Yan, Pei Yan, Shengzhou Xiong, Xuanyu Xiang, and Yihua Tan. Monocd: Monocular 3d object detection with complementary depths. In *CVPR*, pages 10248–10257, 2024.
- [49] Yan Yan, Yuxing Mao, and Bo Li. Second: Sparsely embedded convolutional detection. *Sensors*, 18(10):3337, 2018.
- [50] Lei Yang, Xinyu Zhang, Jun Li, Li Wang, Minghan Zhu, Chuang Zhang, and Huaping Liu. Mix-teaching: A simple, unified and effective semi-supervised learning framework for monocular 3d object detection. *TCSVT*, 33(11):6832–6844, 2023.
- [51] Yiran Yang, Dongshuo Yin, Xuee Rong, Xian Sun, Wenhui Diao, and Xinming Li. Beyond the limitation of monocular 3d detector via knowledge distillation. In *ICCV*, pages 9077–9086, 2023.
- [52] Tianwei Yin et al. Center-based 3d object detection and tracking. In *CVPR*, pages 11784–11793, 2021.
- [53] Renrui Zhang, Han Qiu, Tai Wang, Ziyu Guo, Ziteng Cui, Yu Qiao, Hongsheng Li, and Peng Gao. Monodeptr: Depth-guided transformer for monocular 3d object detection. In *CVPR*, pages 9155–9166, 2023.
- [54] Shengchao Zhou, Weizhou Liu, Chen Hu, Shuchang Zhou, and Chao Ma. Unidistill: A universal cross-modality knowledge distillation framework for 3d object detection in bird’s-eye view. In *CVPR*, pages 5116–5125, 2023.
- [55] Yunsong Zhou, Hongzi Zhu, Quan Liu, Shan Chang, and Minyi Guo. Monoatt: Online monocular 3d object detection with adaptive token transformer. In *CVPR*, pages 17493–17503, 2023.
- [56] Xizhou Zhu, Han Hu, Stephen Lin, and Jifeng Dai. Deformable convnets v2: More deformable, better results. In *CVPR*, pages 9308–9316, 2019.

# MonoTAKD: Teaching Assistant Knowledge Distillation for Monocular 3D Object Detection

## Supplementary Material

Due to the page constraint of the main paper, we provide more quantitative and qualitative results in this supplementary material, which is organized as follows:

- Dataset description of KITTI raw set in Section A.
- The implementation and training details for KITTI and nuScenes datasets are documented in Section B.
- More qualitative results for MonoTAKD in Section C.
- More ablation studies for MonoTAKD in Section D.
- Quantitative results for MonoTAKD in Section E.

### A. Datasets

**KITTI Raw.** The KITTI Raw dataset includes approximately 48K unlabeled data used for semi-supervised training. Following [12, 32], we train on the Eigen clean subset (22K) of the raw KITTI dataset and evaluate on the KITTI test set (3,769). The evaluation metric and the implementation of KITTI raw are the same as the KITTI3D dataset.

### B. Implementation Details

For the KITTI dataset, we use a pre-trained Second [49] as the LiDAR-based teacher. Both the camera-based teaching assistant and camera-based student are derived from CaDDN [35], using ResNet50 as their backbone. In addition, we use PointPillar [22] as the BEV detector.

Initially, we trained the teaching assistant model for 30 epochs. Then, a pre-trained teacher model and a frozen teaching assistant model are used to train the student model for another 60 epochs. Training is performed with an NVIDIA Titan XP GPU in an end-to-end manner. We set the batch size to 2, and the learning rate is  $2e^{-4}$  with the one-cycle learning rate strategy. The IoU thresholds for the Car, Pedestrian, and Cyclist categories are 0.7, 0.5, and 0.5, respectively. As for the discrete depth bins  $D$ , we set  $D$  to 120, and the minimum and maximum depths are set to 2.0 and 46.8 meters, respectively.

In the case of the nuScenes dataset, we adopt a pre-trained CenterPoint [52] as the LiDAR-based teacher and use BEVDepth [24] for both the teaching assistant and the student. Due to a higher resolution and a larger model size, we set the batch size to 8 and trained the models with eight NVIDIA V100 GPUs. We set the learning rate of  $2e^{-4}$  with a multi-step learning rate decay schedule and a decay rate of 0.1 and train the model for 25 epochs.

### C. More Qualitative Results

**Results for Pedestrian and Cyclist.** We present a detailed comparison with other state-of-the-art methods for the non-car categories on the KITTI test set. Table C1 demonstrates that MonoTAKD outperforms other methods not only in the Car category but also in the Pedestrian and Cyclist categories. This success indicates that the approach is well-suited for a wide range of autonomous driving applications, including tasks such as trajectory prediction.

**Results on KITTI raw.** To improve the transferability and to generalize the application of MonoTAKD on real-world scenes, we explore the performance of MonoTAKD in a semi-supervised manner. As illustrated in Table C2, our MonoTAKD surpasses CMKD by 1.31/3.85, 2.57/6.49, and 1.50/5.68 in  $AP_{3D}/AP_{BEV}$  across all three difficulty levels, respectively.

Owing to MonoTAKD’s outstanding performance in semi-supervised settings, it is evident that our distillation method adeptly extracts valuable 3D features from unlabeled data. Thus, MonoTAKD can provide comprehensive guidance for the student model across all difficulty levels.

### D. More Ablation Studies

Here, we discuss the backbone choices on the KITTI dataset and the detector choices on the nuScenes dataset.

**Backbone choices on KITTI.** We analyze the backbone choice of our MonoTAKD in Table D3. According to Table D3, Swin-T, a transformer-based backbone, exhibits higher FLOPs and underperforms in both speed and accuracy. We believe the performance drop is because of the heterogeneity of the architecture between teacher and student (CNN and Transformer). Conversely, MobileNetV3, a lightweight backbone, excels in speed and efficiency with lower FLOPs but has a trade-off with lower accuracy.

After comparing ResNet50 and ResNet101, we determined that ResNet50 is the optimal backbone for the student model, delivering enhanced performance with higher AP, improved FPS, and reduced FLOPs. This finding highlights that in Mono3D tasks, a larger or more complex backbone does not necessarily translate to better performance. Note that, we only compare the FLOPs of the backbone. The total FLOPs can be found in Table 6.

**Detector choices on nuScenes.** As shown in Table D4, we report the NDS and mAP scores of CaDDN. The detector originally was developed on the KITTI dataset. Through the experiment, the performance of CaDDN on the nuScenes

Table C1. Experimental results for Pedestrian and Cyclist categories on the KITTI *test* set. We use **bold** and underline to indicate the best and the second-best results, respectively.

Method	Venue	Pedestrian $AP_{3D}/AP_{BEV}$			Cyclist $AP_{3D}/AP_{BEV}$		
		Easy	Mod.	Hard	Easy	Mod.	Hard
MonoPSR [21]	CVPR 2019	6.12/7.24	4.00/4.56	3.30/4.11	8.37/9.87	4.74/5.78	3.68/4.57
MonoATT [55]	CVPR 2023	10.55/11.63	6.66/7.40	5.43/6.56	5.74/6.73	3.68/4.44	2.94/3.75
Cube R-CNN [2]	CVPR 2023	11.17/11.67	6.95/7.65	5.87/6.60	3.65/5.01	2.67/3.35	2.28/3.32
CaDDN [35]	CVPR 2021	12.87/14.72	8.14/9.41	6.76/8.17	7.00/9.67	3.41/5.38	3.30/4.75
DD3D [30]	ICCV 2021	13.91/15.90	9.30/10.85	8.05/8.05	2.39/3.20	1.52/1.99	1.31/2.39
MonoNerd [47]	ICCV 2023	13.20/15.27	8.26/9.66	7.02/8.28	4.79/5.24	2.48/2.80	2.16/2.55
MonoUNI [18]	NeurIPS 2023	<u>15.78/16.54</u>	<u>10.34/10.90</u>	<u>8.74/9.17</u>	7.34/8.25	<u>4.28/5.03</u>	<u>3.78/4.50</u>
OccupancyM3D [33]	CVPR 2024	<u>14.68/16.54</u>	9.15/10.65	7.80/9.16	7.37/8.58	3.56/4.35	2.84/3.55
<b>MonoTAKD</b>	-	<b>16.15/19.79</b>	<b>10.41/13.62</b>	<b>9.68/11.92</b>	<b>13.54/16.90</b>	<b>7.23/9.42</b>	<b>6.86/8.29</b>

Table C2. Experimental results on the KITTI *test* set for the Car category, leveraging unlabeled data. We use **bold** and underline to indicate the best and the second-best results, respectively.

Method	Venue	Extra Data	$AP_{3D}$			$AP_{BEV}$		
			Easy	Mod.	Hard	Easy	Mod.	Hard
LPCG [32]	ECCV 22	Raw	25.56	17.80	15.38	35.96	24.81	21.86
Mix-Teaching [50]	CSVT 23		26.89	18.54	15.79	35.74	24.23	20.80
CMKD [12]	ECCV 22		<u>28.55</u>	<u>18.69</u>	<u>16.77</u>	<u>38.98</u>	<u>25.82</u>	<u>22.80</u>
<b>MonoTAKD</b>	-	Raw	<b>29.86</b>	<b>21.26</b>	<b>18.27</b>	<b>43.83</b>	<b>32.31</b>	<b>28.48</b>

Table D3. Generalization of MonoTAKD using different backbones.

Backbone	Speed (FPS)	FLOPs (G)	$AP_{3D}$		
			Easy	Mod.	Hard
Swin-T	5.8	16.7	31.57	19.33	17.65
MobileNetV3	13.8	3.4	26.11	16.87	13.92
ResNet101	9.2	4.3	33.07	21.54	19.16
<b>ResNet50</b>	<b>11.9</b>	<b>4.1</b>	<b>34.36</b>	<b>22.61</b>	<b>19.88</b>

dataset is subpar, which we attribute to the different settings between the datasets it trained on: (1) **Monocular camera**. In the KITTI dataset, a single 2D image is utilized as the input. Thus, most approach primarily focuses on generating accurate depth maps to reconstruct 3D representations or on extracting valuable 3D information from unsupervised data. (2) **Multi-view camera**. The nuScenes dataset uses multi-view images as input. Therefore, most methods specialize in integrating temporal information [17, 25] to enhance 3D representations. Therefore, the common detectors [14, 28] that excel on nuScenes are rarely reported on the KITTI 3D dataset due to under-performing results.

Furthermore, the benchmarks of KITTI and nuScenes datasets reveal distinct top-performing methods, emphasizing the need for detectors to specialize in either monocular or multi-view camera settings. As a result, we implement our MonoTAKD on BEVFormer and BEVDepth as the student models to validate the effectiveness of our approach.

Table D4. Experimental results on the nuScenes *val* set. We use **bold** and underline to indicate the best and the second-best results, respectively.

Method	NDS $\uparrow$	mAP $\uparrow$
PETrv2 [27]	0.456	0.349
P2D [19]	0.514	0.420
CaDDN	0.396	0.300
+ MonoTAKD	0.427	0.327
BEVFormer [25]	0.423	0.352
+ MonoTAKD	0.490	0.392
BEVDepth [24]	0.440	0.317
+ MonoTAKD	<b>0.537</b>	<b>0.430</b>

## E. Qualitative Results

We visualize both the 3D object and BEV detection results of MonoTAKD on KITTI in Fig. E1. We compare our performance with the SOTA KD method, CMKD [12], and the SOTA depth-guided method, MonoDETR [53]. MonoTAKD comparatively has the best-fitted bounding box size estimation and the most accurate 3D localization among the three methods.

Lastly, Fig. E2 presents the BEV features of the teacher, teaching assistant (TA), and the student. Notice the student’s BEV image exhibits distortion and blurriness. However, with the help of SAM and FFM modules, the student’s BEV features successfully align more closely to resemble the BEV LiDAR features. This visual comparison illustrates how the proposed approaches collectively contribute to improving the student’s 3D perception.



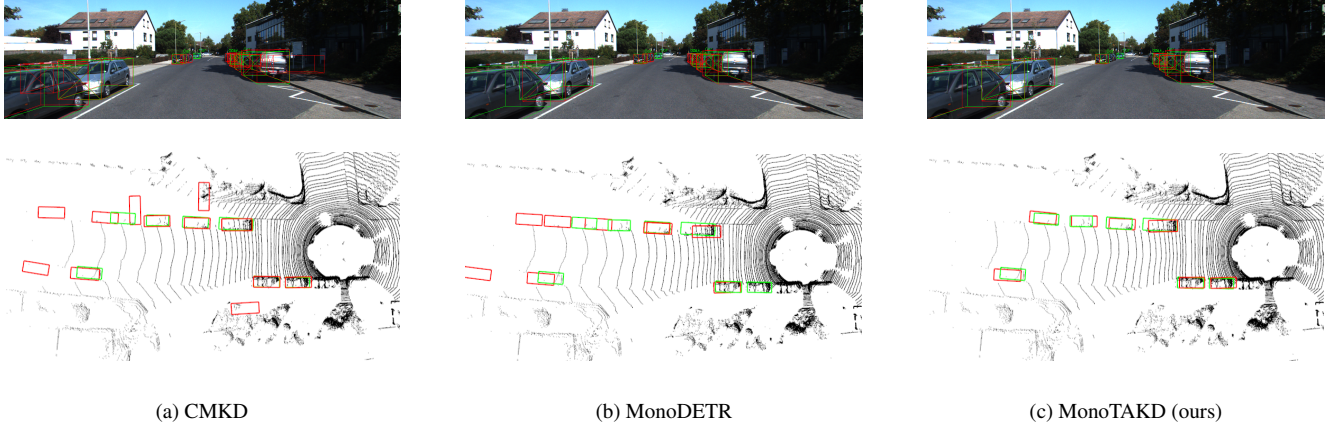


Figure E1. Qualitative results on KITTI *val* set for the Car category. We compare the qualitative results among CMKD [12], MonoDETR [53], and our proposed MonoTAKD. The first and second rows represent detection results from a camera frontal view and a BEV, respectively. We use green and red boxes to indicate the ground truth and prediction bounding boxes.

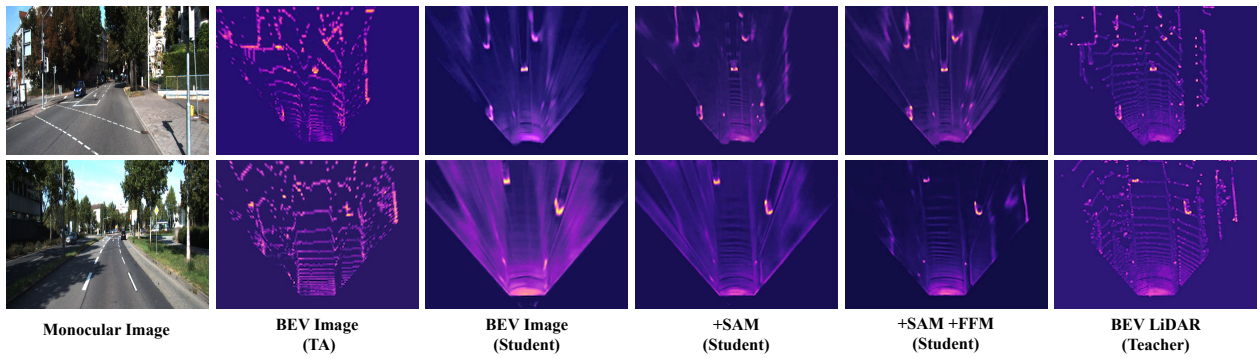


Figure E2. Visualization of the BEV features from the teacher, teaching assistant (TA), and the two distillation branches of the student model on KITTI *val* set.